A 2.4 GHz Wireless Temperature Sensor with 0.93 °C Precision Designed in 130 nm CMOS Technology for Internet of Things Applications

Hugo Dias Gilo, and Francisco de Assis Brito-Filho

***Abstract*—Temperature sensors are present in many applications within the context of the Internet of Things, such as monitoring people, equipment, homes, industries, among others. Some of these portable devices need low power consumption, be compact, and have a linearity range for their application. Therefore, this work proposes a wireless temperature sensor developed in 130-nanometer CMOS technology, designed to operate in the 2.4 GHz ISM band. The wireless sensor was developed using exclusively open-source EDA tools and the Skywater 130 nm openPDK. The device's linearity was evaluated between -50°C to 200°C, demonstrating a maximum inaccuracy of 0.93 °C in a range from 12.0 °C to 144.0 °C, while consuming only 1.6 mW and occupying an area of 0.028 mm², including the RF block. Additionally, this work was compared with sensors reported in the state of the art and its area and maximum error were smaller.**

Link to graphical and video abstracts, and to code: https://latamt.ieeer9.org/index.php/transactions/article/view/9300

***Index Terms*—Wireless, Temperature Sensor, CMOS, Internet of Things.**

I. Introduction

CURRENTLY, there is a growing integration of electronic devices in the context of the Internet of Things (IoT). These devices communicate with each other, forming an interconnected network, and autonomously share data. The number of devices connected to the IoT increases each year, with projections pointing to 75.44 billion by 2025 and a trajectory of continuous growth [1].

In addition to interconnection, devices in the context of IoT tend towards miniaturization, aiming for lower cost and portability. For this purpose, semiconductor mass production is essential. In 2019, the utilization rate of semiconductor production lines reached about 90%, driven by the growing demand for electronic applications, development of more autonomous circuits, automated applications (including IoT), and vehicle connectivity. Even with the impact of the pandemic, the average industrial chip capacity remained above 90% [2].

Therefore, optimizing integrated circuit production is crucial to ensure efficient supply chains and drive technological advancements.

The associate editor coordinating the review of this manuscript and approving it for publication was Roberto S. Murphy (*Corresponding author: Hugo Dias Gilo*).

Hugo Dias Gilo, and F. D. A. Brito-Filho are with Universidade Federal Rural do Semi-Arido, Brazil (e-mails: hugo.gilo@alunos.ufersa.edu.br, and francisco.brito@ufersa.edu.br).

To enable portability and reusability of chips in IoT applications, these circuits need to be compact and have low power consumption. This may require simpler circuit topologies. Among the variety of available components, temperature sensors stand out, being of utmost importance for the composition of multi-monitoring systems [3].

This work presents an integrated wireless temperature sensor designed to address the specific needs of IoT devices and applications, prioritizing portability, low power consumption, and compact form factor. The circuits were analyzed and designed to operate within the widely adopted 2.4 GHz ISM frequency band. The linearity of the sensor was validated in a broad temperature range of -50°C to 200°C. A post-layout analysis was performed that compared the performance of our temperature sensor with state-of-the-art solutions in terms of inaccuracy, linear range, area occupancy, and power consumption.

This project leveraged open-source tools throughout its entire lifecycle, including design, simulation, and post-layout verification. Tools such as ASITIC, XSchem, Ngspice, Magic, and Netgen were employed. This approach aligns with the growing movement towards democratizing integrated circuit design. The increasing adoption of open-source EDA tools has facilitated the development of complete ASIC design flows, as evidenced by recent advancements [4]. The proposed circuit was designed using the open-source Skywater 130 nm CMOS PDK [5].

II. Methodology

In this section, the computational tools used for modeling and simulation, the proposed device, and the detailed description of each of its blocks individually will be presented.

A. Tools and Analysis

The tools used (Fig. 1) covered all stages of the integrated circuit design flow, all of which were open source. Xschem (version 3.1.0) was used for schematic capture and SPICE file generation, which were later simulated in Ngspice (version 37+). Magic VLSI (version 8.3.329) was used for layout implementation and parasitic extraction, as well as physical DRC (Design Rules Check) verification.

Netgen (version 1.5.234) was used for LVS (Layout Versus Schematic) verification and ASITIC (version X11R6) was used to inductor modeling. The tool also generates files that can be

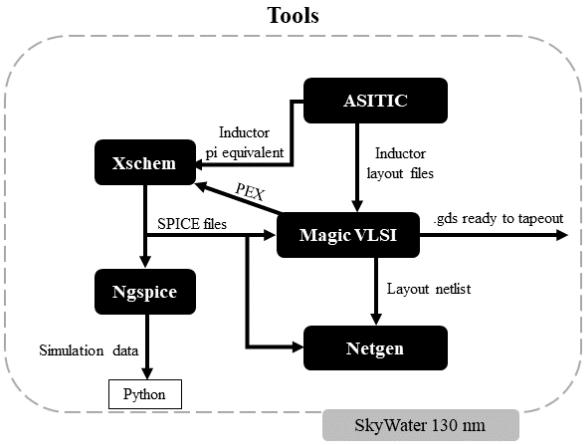

Fig. 1. A flowchart illustrating the tools used throughout the process, from pre-layout to post-layout simulations, as well as post-processing data using Python.

exported to the final layout and equivalent pi models of the inductors to be used in simulations.

To analyze the device's performance, temperature sweep simulations were conducted to verify the sensor's linearity within the range of -50°C to 200°C. Additionally, transient simulations were performed at temperatures of 10°C, 35°C, and 60°C to observe the signal behavior. These values were chosen as they represent key central temperatures relevant for applications such as environmental monitoring systems [6], smart agriculture [7], human thermal comfort [8], industries [9], among others.

Additionally, the collected data were processed using Python programs to: generate discrete Fast Fourier Transforms (FFTs) using the *numpy* library to verify the frequency at the output of the ASK modulator; and perform linear regressions with the *sklearn.linear_model* library to calculate linearity intervals and temperature measurement errors.

Finally, energy consumption, area occupation, linear range, and inaccuracy were extracted for comparison with other CMOS temperature sensors present in the state of the art.

B. Proposed Circuit

The proposed wireless temperature sensor has the configuration shown in Fig. 2. The PTAT (Proportional to Absolute Temperature) sensor generates a voltage signal that passes through a buffer and reaches a mixed-signal part, composed of a second-order continuous-time $\Sigma\Delta$ modulator to convert the analog signal into digital pulses. These digital pulses are then converted into modulated signals in the 2.4 GHz ISM band by an ASK (Amplitude Shift-Keying) modulator, whose topology is analyzed in [10]. All information regarding circuit specification, simulation, and layout, including source files, can be found in the GitHub repository [11].

1) PTAT (Proportional to Absolute Temperature): The PTAT used in this work was described by [12], which proposes a modification compared to the PTAT by [13]. This modification involves using a PMOS transistor as the main element of the sensor, as it is naturally isolated by the n-well when

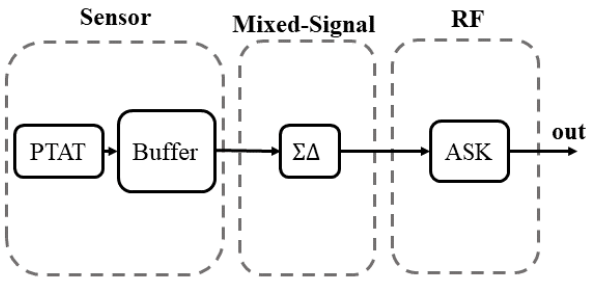

Fig. 2. Block diagram of the proposed wireless temperature sensor.

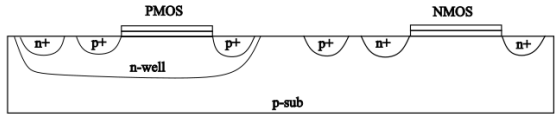

(a) Standard manufacturing process.

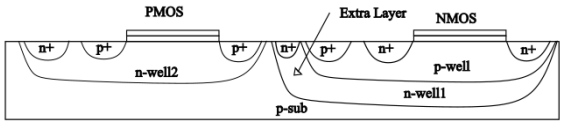

(b) Triple n-well manufacturing process.

Fig. 3. The standard and triple n-well CMOS manufacturing processes cross sections.

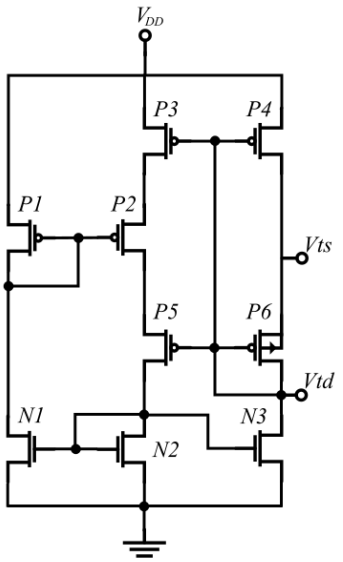

Fig. 4. PTAT Circuit Schematic.

fabricated using a standard manufacturing process (Fig. 3a). If this main sensor were of the NMOS type, additional layers would be required, as in the Triple n-well process (Fig. 3b).

The PTAT schematic is presented in Fig. 4, where transistors P1 and P2 are operating in weak inversion, P3 in the linear region, P4 in saturation, and transistor P6 is isolated with the substrate connected to its source. Transistors N1, N2, and N3 are NMOS transistors associated in series and parallel to form a current mirror network and increase the output conductance.

The Equations (1), (2) and (3) described in [12] were used to calculate V_{ts} and TC (Temperature Coefficient), respectively:

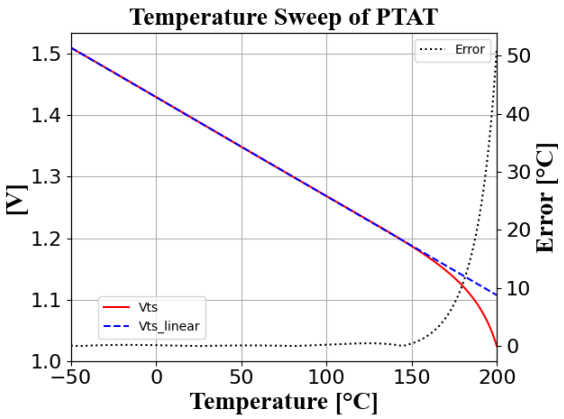

Fig. 5. Temperature Sweep of the PTAT.

$$V_{ts} = V_{DD} - BT \tag{1}$$

$$TC = \frac{\partial V_{ts}}{\partial T} = -B \tag{2}$$

$$B = 2\eta \left(\frac{k}{q}\right) \left(\frac{W3}{L3}\right) \left(\frac{L4}{W4}\right) \ln\left(\frac{W2}{L2}\right) \left(\frac{L1}{W1}\right) \tag{3}$$

where W is the width, L is the length of the transistor channel, η is a process-dependent parameter, k is the Boltzmann constant, q is the charge of an electron, T is the temperature in Kelvins, and V_{DD} is the supply voltage.

In Fig. 5, it can be observed that both Vts and Vtd remain approximately linear in the range of 10°C to 150°C, with a Temperature Coefficient (TC) of 1.64 mV/°C. After around 150°C, Vts starts to decay abruptly and loses its linear characteristics.

To measure the error, a linear line Vts_linear was created through linear regression, aiming to compare it with Vts and estimate error values in °C. The results are shown in Table I.

TABLE I
MAXIMUM ABSOLUTE ERRORS OF THE PTAT

Maximum absolute error (°C)	Range (°C)
0.001	-44.9 to 80.1
0.01	-45.4 to 144.6
0.1	-50.0 to 145.9
1.0	-50.0 to 154.7

The Table II contains a summary of the PTAT specifications.

TABLE II
PTAT SPECIFICATIONS

Parameter	Value
TC	-1.62 mV/°C
Out	1.18 V to 1.51 V
Inaccuracy (-50 °C to 150 °C)	≤0.48 °C

2) Buffer: Between the PTAT and the sigma-delta modulator, a unity gain buffer Fig. 6 was inserted with an open-loop gain approximately equal to that of a single-stage amplifier, as seen in [14]. A compensation capacitor C_C was added to ensure more stability at the buffer output and prevent oscillations stemming from its connection to the sigma-delta modulator.

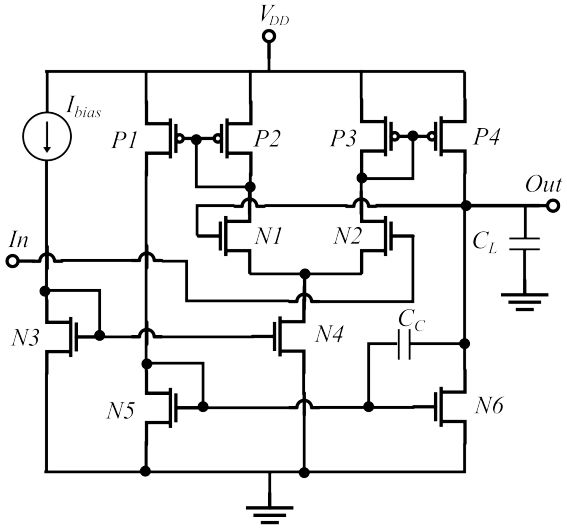

Fig. 6. Buffer Circuit Schematic.

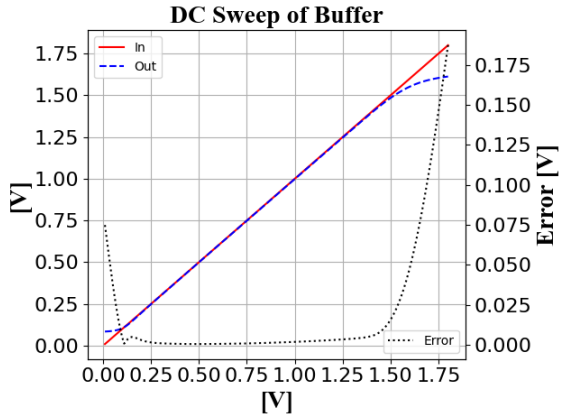

Fig. 7. DC Sweep analysis of the input signal of the Buffer.

The Fig. 7 illustrates the DC simulation of the buffer with a load capacitance C_L set to 4 pF. The results indicate that the buffer accurately replicates the input signal *In* to the output *Out* within the range of 0.1 V to 1.48 V. However, without considering temperature variations, a limitation in the PTAT+buffer assembly becomes apparent. The buffer's linearity deteriorates as the output approaches 1.5 V, which corresponds to -50 °C in the PTAT, as shown in Fig. 5.

In Table III, a summary of the buffer specifications is provided.

TABLE III
BUFFER SPECIFICATIONS

Parameter	Value
Slew Rate	0.092 V/μs
Cut-off Frequency	14.6 MHz
Linear operating range	0.1 V to 1.45 V

3) Sigma-Delta Modulator: The ADC (Analog-to-Digital Converter) that converts the analog signal coming from the PTAT+Buffer to digital pulses is a second-order continuous-time sigma-delta modulator (Figs. 8a and 8b).

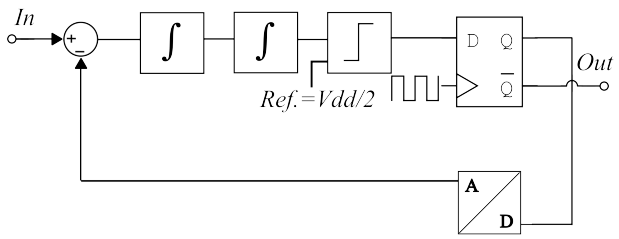

(a) Block diagram.

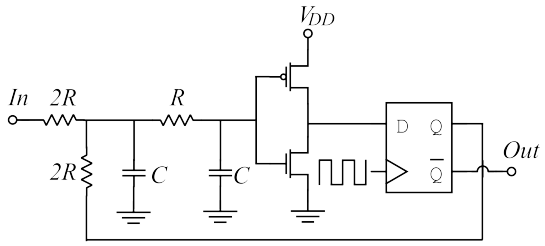

(b) Schematic.

Fig. 8. Representations of the sigma-delta modulator. (a) Block diagram. (b) Schematic.

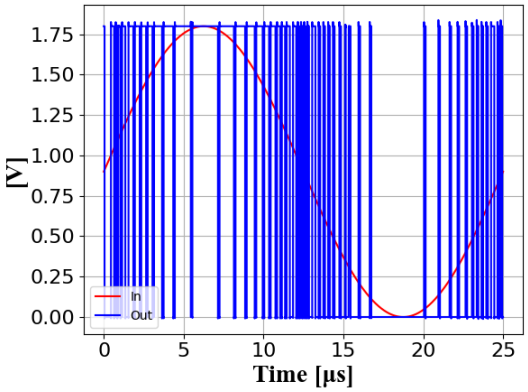

Fig. 9. Transient simulation of the sigma-delta modulator.

The addition of another integrator to the sigma-delta modulator was necessary to increase the conversion resolution, considering that the sensor has a variation on the order of mV to change 1°C, contrasting with the total supply range from 0 to 1.8 V [5].

To verify the operation of the sigma-delta modulator, a transient simulation of the modulator output when subjected to a sinusoid at the input is performed (Fig. 9). It is observed that the digital pulses Out have a higher duty cycle as the voltage In increases and vice-versa.

In Table IV, there is a summary of the specifications of the sigma-delta modulator.

TABLE IV
SIGMA-DELTA SPECIFICATIONS

Parameter	Value
Input and Output Range	0.0 V to 1.8 V
Oversampling Frequency	10 MHz

4) ASK (Amplitude Shift-Keying) Modulator: To transmit the digital pulses from the sigma-delta modulator, an ASK

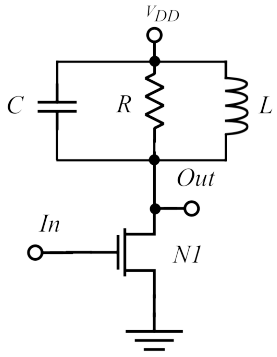

Fig. 10. ASK Modulator Circuit Schematic.

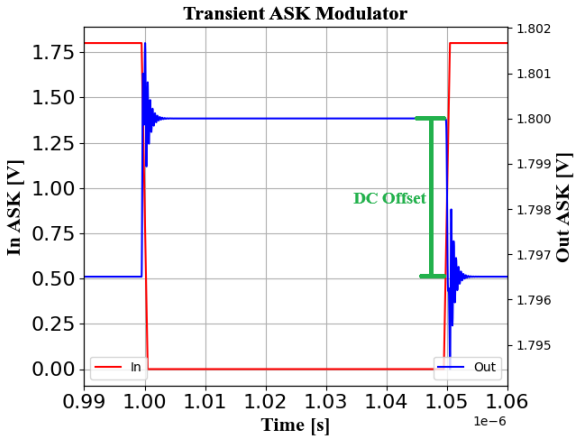

Fig. 11. Transient simulation of the ASK modulator.

modulator (Fig. 10) was designed, containing an NMOS for switching and an RLC circuit to generate the 2.4 GHz carrier.

When there is a voltage switching at the input In, underdamped oscillation pulses Out are generated (Fig. 11) with the resonance frequency of the tank circuit, as observed in its discrete post processed FFT in Fig. 12. The Output Impedance was used in order to carry out external matching for test purposes.

In Fig. 11, it can be observed that during the switching in the digital signal at In ASK, there is a manifestation of an underdamped oscillatory signal and a DC offset relative to the 1.8 V supply of about 3 μV at the output of the device Out. This behavior, along with other effects resulting from the internal resistance of the inductors, which is incorporated into their pi model, was analyzed by [10]. On the other hand, Fig. 12 demonstrates the presence of the fundamental component in the ISM band of 2.4 GHz, with an amplitude of approximately 350 μV. Therefore, the ASK exhibited the expected performance.

In Table V, there is a summary of the specifications of the ASK modulator.

TABLE V
ASK MODULATOR SPECIFICATIONS

Parameter	Value
Carrier frequency	2.4 GHz
Output Impedance	200 + j13.54 Ω

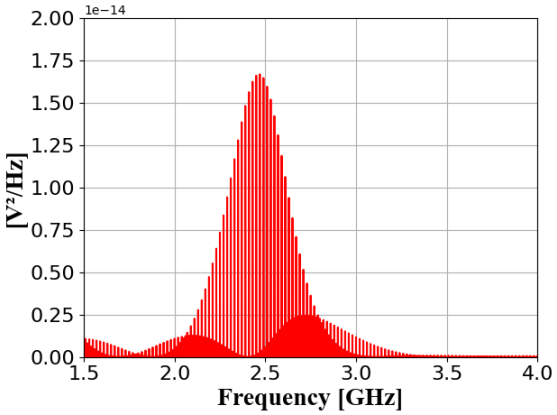

Fig. 12. FFT of the ASK modulator.

III. Results

In this section, simulations of the device will be presented first, observing the operation of all its blocks. Then, the layout and its integration into a *Harness* will be shown. Finally, a comparison with other temperature sensors from the literature will be conducted.

A. Simulations

With the complete device, a temperature sweep was done to observe the PTAT+Buffer assembly, aiming to verify if temperature variations could affect the copying of the PTAT voltage to the sigma-delta modulator by the buffer. For this purpose, the *ss* and *ff* corners were considered, together with the typical case (*tt*), to analyze if there would still be a linear behavior even with variations in the manufacturing process (Fig. 13).

It is noted that the Vts (PTAT output voltage) has a DC offset with respect to the buffer output Out_buff for both the ff corner (Fig. 13a) and tt (Fig. 13b). Nevertheless, in all three cases, the buffer output exhibited linear behavior within a certain region. This can be verified with the Maximum Absolute Error, which compares the buffer output Out_Buff with a linear line Out_Buff_linear. These intervals are shown in Table VI.

TABLE VI
Maximum Absolute Error for Different Temperature Intervals

Max. absolute error (°C)	Range (°C) ff	tt	ss
0.001	33.8 to 81.9	30.5 to 70.9	0.8 to 84.2
0.01	33.2 to 83.0	30.0 to 73.3	0.7 to 168.2
0.1	28.3 to 91.8	26.3 to 119.7	-1.0 to 168.9
1	9.5 to 126.0	11.5 to 144.6	-11.8 to 171.1

It's possible to observe that the variations in corners generate regions of linearity for different values of maximum absolute errors in the device. However, for the highest precision (0.001 °C), it still encompasses the region near the human body temperature (35°C), for example, which indicates an increased reliability of the component, even with manufacturing variations.

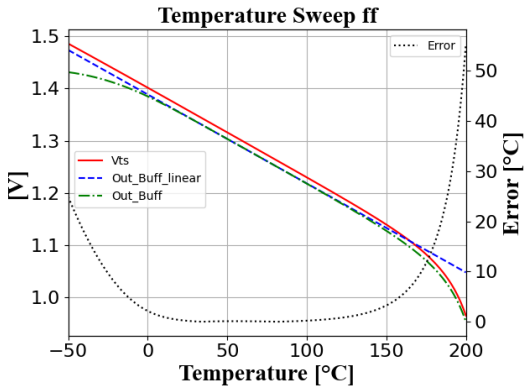

(a) ff Corner.

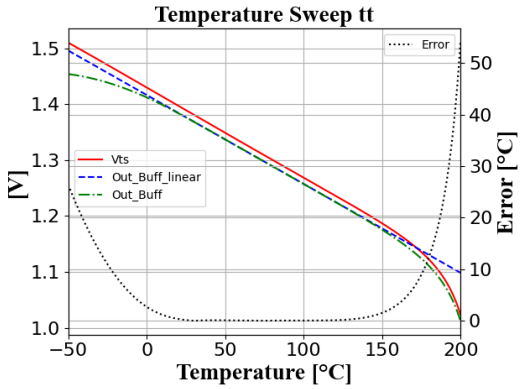

(b) tt.

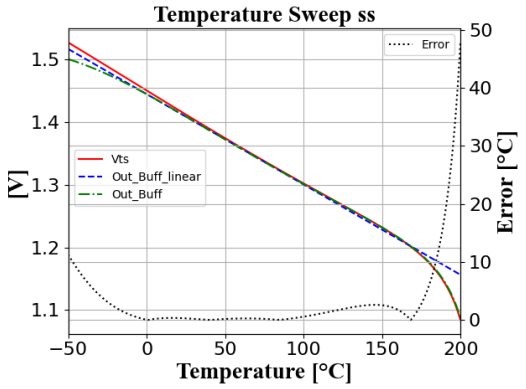

(c) ss Corner.

Fig. 13. A Temperature Sweep of the device. (a) ff Corner. (b) tt. (c) ss Corner.

After analyzing the temperature variation, transient simulations were conducted at temperatures of 10°C, 35°C, and 60°C to analyze: the voltage (Vts) coming out of the PTAT, its copy by the buffer; the sigma-delta (Fig. 14); and the ASK signals, which had results similar to Figs. 11 and 12.

For different temperatures, the output of the PTAT Vts, and consequently, the output of the buffer Out_Buff, changed, decreasing their values with increasing temperature. This is consistent with the design, as the PTAT has a negative temperature coefficient TC. This change results in a different sequence of pulses presented at the output of the sigma-delta modulator

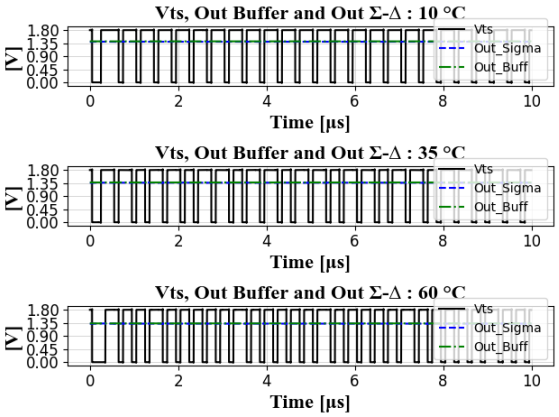

Fig. 14. Transient simulation of the device to observe Vts, Out Buffer, and Out sigma-delta at temperatures of 10 °C, 35 °C, and 60 °C.

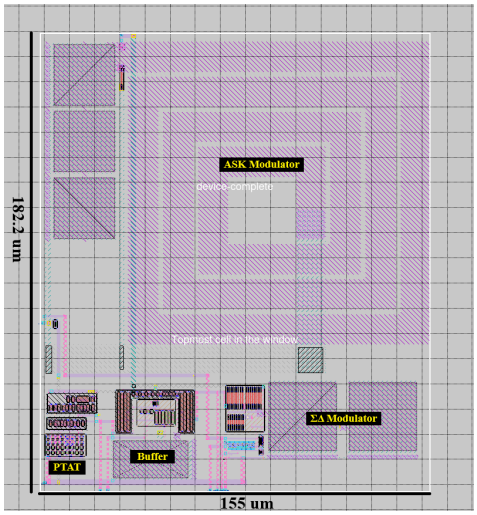

Fig. 15. Layout of the complete device.

Out_Sigma. For 10 °C, the pulses are approximately equal. However, at 35 °C, there are two wider pulses followed by a shorter one. And, at 60 °C, there is one wider pulse followed by five shorter pulses. This pattern can be detected in the demodulator of the receiving device.

B. Layout

The layout of the device is presented in Fig. 15, where various many techniques have been employed, such as interdigitation and separation of transistors into "fingers", with the purpose of avoiding mismatches and ensuring the correct functioning of the device.

The device was integrated into the Caravel Harness provided by [15] for fabrication and testing. This Harness includes a SoC (System-on-Chip) and an available user area of 10.33 mm². In this area, it is possible to incorporate the layout of the device, as well as to have support for various analog and digital IOs, as well as ESD (Electrostatic Discharge) protection systems, among other functionalities.

Each device pin was connected to a suitable Harness pin. Separate power supplies were used for digital and analog (including RF) sections, while sharing a common ground.

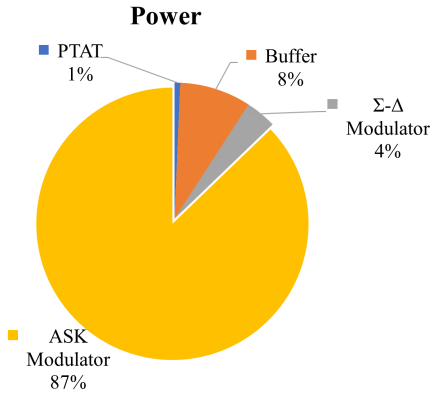

Fig. 16. Power consumption of the device (27 °C).

C. Comparison with Other Temperature Sensors

Table VII shows some temperature sensors present in the state of the art. It is important to highlight that this work includes an additional block absent in the others: the RF block (ASK modulator), which represents 75% of the total area and consumes 87% of the energy (Fig. 16). Power consumption was estimated by measuring current at 27°C with a 10 MHz clock and calculating the mean energy consumption. However, without it, that is, containing only the analog and analog-to-digital modulation parts, the device shown a smaller area than all other sensors and lower energy consumption than [16] and [19]. Even including the RF part, this work presented a smaller area than [16], [18], [19] and [21], as well as lower consumption than [16].

IV. Conclusions

The proposed temperature sensor with wireless communication was validated through post-layout simulations using 130-nanometer CMOS technology. The results demonstrated the proper operation of the device, generating a voltage signal that varies linearly with temperature and is modulated to high-frequency signals in the 2.4 GHz ISM band, thus enabling temperature measurement through wireless transmission.

The complete circuit consumes only 1.6 mW and has an area of 0.028 mm², smaller than most of the other compared sensors. Its maximum error was 0.93°C for a temperature range between 12°C and 144°C, which is lower than all analyzed circuits. These results highlight its viability and relevance in the context of the Internet of Things. Additionally, all the design steps were performed using open-source tools, contributing to the emerging movement of democratizing integrated circuit design. Moreover, all the blocks are modular and can be customized.

As a suggestion for future work, it is recommended to consider adding an impedance matching network to the output of the ASK modulator to improve device matching with an antenna and an RF amplifier. Furthermore, a bandgap reference could be included to generate internal signals and serve as a current source to power the buffer.

TABLE VII
COMPARISON WITH STATE-OF-THE-ART TEMPERATURE SENSORS

Sensor	Range (°C)	Inaccuracy (°C)	Area (mm²)	Power (μW)	Node (nm)
This	12 to 144 [2]	+0.93	0.007 (0.028)[1]	209,9 (1600)[1]	130
[16]	-40 to 100	0.5	0.682	15400	180
[17]	0 to 95	-0.35/+0.58	0.00932	4.043	65
[18]	-55 to 125	±0,15	0.25	0.81	180
[19]	-40 to 175	±1.0	0.42	300	180
[20]	-20 to 100	-0.072/+0.082	0.0107/0.0282	0.036	180
[21]	-40 to 90	+0.75/-0.92	0.63	25.4	130

[1] Considering the RF block (ASK modulator).
[2] Refer to Table VI in the tt to find the other ranges of maximum errors.

REFERENCES

[1] STATISTA. IoT: number of connected devices worldwide 2012-2025 | Statista. Available at: <https://www.statista.com/statistics/471264/iot-number-of-connected-devices-worldwide/>. Accessed: Sep. 25, 2024.

[2] HARRIS, MARK. These 5 Charts Help Demystify the Global Chip Shortage. IEEE Spectrum. Available at: https://spectrum.ieee.org/global-chip-shortage-charts. Accessed on: 1st May 2022.

[3] D. Blaauw et al., "IoT design space challenges: Circuits and systems," 2014 Symposium on VLSI Technology (VLSI-Technology): Digest of Technical Papers, Honolulu, HI, USA, 2014, pp. 1-2, doi: 10.1109/VLSIT.2014.6894411.

[4] R. T. Edwards, M. Shalan and M. Kassem, "Real Silicon Using Open-Source EDA," in IEEE Design Test, vol. 38, no. 2, pp. 38-44, April 2021, doi: 10.1109/MDAT.2021.3050000.

[5] SKY130. SkyWater PDK. Available at: https://skywater-pdk.readthedocs.io/en/main/. Accessed on: Sep. 25, 2024.

[6] F. Zonzini et al., "Structural health monitoring and prognostic of industrial plants and civil structures: A sensor to cloud architecture," IEEE Instrum. Meas. Mag., vol. 23, no. 9, pp. 21–27, Dec. 2020, doi: 10.1109/MIM.2020.9289069.

[7] K. Fizza, P. P. Jayaraman, A. Banerjee, D. Georgakopoulos, and R. Ranjan, "Evaluating Sensor Data Quality in Internet of Things Smart Agriculture Applications," IEEE Micro, vol. 42, no. 1, pp. 51–60, Jan.-Feb. 2022, doi: 10.1109/MM.2021.3137401.

[8] Izhar et al., "Single-Chip Integration of CMOS Compatible Mems Temperature/Humidity and Highly Sensitive Flow Sensors for Human Thermal Comfort Sensing Application," 2021 21st International Conference on Solid-State Sensors, Actuators and Microsystems (Transducers), Orlando, FL, USA, 2021, pp. 1219-1222, doi: 10.1109/Transducers50396.2021.9495565.

[9] S. I. Nahid and M. M. Khan, "Toxic Gas Sensor and Temperature Monitoring in Industries using Internet of Things (IoT)," 2021 24th International Conference on Computer and Information Technology (ICCIT), Dhaka, Bangladesh, 2021, pp. 1-6, doi: 10.1109/ICCIT54785.2021.9689802.

[10] Gilo, H. D. and F. A. Brito-Filho, "Influência da resistência interna de indutores quadrados em moduladores ASK em CMOS de 130 nanômetros," in Simpósio Brasileiro de Micro-ondas e Optoeletrônica (SBMO), 2022. Available at: https://www.sbmo.org.br/sbmo/2022/noticia/58/anais-do-20o-simposio-brasileiro-de-micro-ondas-e-optoeletronica. Accessed on: Sep. 25, 2024.

[11] Gilo, H. D. temp-sensor. Available at: https://github.com/hugodiasg/temp-sensor. Accessed on: 26th January 2023.

[12] J. M. C. Dantas, H. J. B. Costa, J. P. M. Dantas, F. A. B. Filho, F. R. Sousa and R. C. S. Freire, "Low-Power High-Rensponsivity CMOS Temperature Sensor," 2008 IEEE Instrumentation and Measurement Technology Conference, Victoria, BC, Canada, 2008, pp. 1234-1238, doi: 10.1109/IMTC.2008.4547230.

[13] T. Ohzone, T. Sadamoto, T. Morishita, K. Komoku and H. Iwata, "A CMOS Temperature Sensor Circuit," in IEICETrans. Electron, vol. E90C, no. 4, pp. 895-902, Apr. 2007.

[14] P. E. Allen, D. R. Holberg. CMOS Analog Circuit Design. 2nd Ed., Oxford, New York, 2002.

[15] Efabless Caravel "harness" SoC — Caravel Harness Documentation. Available at: https://caravel-harness.readthedocs.io/en/latest/. Accessed on: Sep. 25, 2024.

[16] R. G. B. Sangalang, S. -H. Luo and C. -C. Wang, "A High Resolution And Wide Range Temperature Detector Using 180-nm CMOS Process," 2023 International Conference on IC Design and Technology (ICICDT), Tokyo, Japan, 2023, pp. 64-67, doi: 10.1109/ICICDT59917.2023.10332257.

[17] Y. Shui and A. Wang, "A 14.17pJ.K2 FoM CMOS Temperature Sensor With 173 μm2 Sensing Core for Remote Sensing in 65-nm CMOS," in IEEE Sensors Journal, vol. 23, no. 22, pp. 27059-27067, 15 Nov.15, 2023, doi: 10.1109/JSEN.2023.3321741.

[18] Z. Tang, S. Pan, M. Grubor and K. A. A. Makinwa, "A Sub-1 V Capacitively Biased BJT-Based Temperature Sensor With an Inaccuracy of ±0.15 °C (3σ) From—55 °C to 125 °C," in IEEE Journal of Solid-State Circuits, vol. 58, no. 12, pp. 3433-3441, Dec. 2023, doi: 10.1109/JSSC.2023.3308554.

[19] H. Liu et al., "An Ultra-High Linear Digitization Temperature Sensor Based on SAR ADC With Common-Mode Temperature Drift Suppression," in IEEE Transactions on Circuits and Systems II: Express Briefs, vol. 71, no. 3, pp. 1047-1051, March 2024, doi: 10.1109/TCSII.2023.3316013.

[20] W. Wang et al., "A 36nW CMOS Temperature Sensor with <0.1K Inaccuracy and Uniform Resolution," 2023 IEEE Symposium on VLSI Technology and Circuits (VLSI Technology and Circuits), Kyoto, Japan, 2023, pp. 1-2, doi: 10.23919/VLSITechnologyandCir57934.2023.10185286.

[21] E. Moisello, C. M. Ippolito, G. Bruno, P. Malcovati and E. Bonizzoni, "A MOS-Based Temperature Sensor With Inherent Inaccuracy Reduction Enabled by Time-Domain Operation," in IEEE Transactions on Instrumentation and Measurement, vol. 72, pp. 1-10, 2023, Art no. 2004110, doi: 10.1109/TIM.2023.3276016.

Hugo Dias Gilo B. Sc. in Electrical Engineering from the Universidade Federal Rural do Semi-Arido (UFERSA) (Brazil) in 2024, with a strong emphasis on research and studies in the field of microelectronics.

Francisco de Assis Brito Filho is a Professor of Electrical Engineering at Federal University of Semiarid Region – UFERSA, in Brazil. He is Ph.D. in Microelectronics from University of Sao Paulo – USP with focus on Radiofrequency Integrated Circuits. Francisco Brito Filho worked from 2009 to 2013 as RFIC Designer on LSITEC Design House before joining UFERSA. He is the head of Microelectronics and Radiofrequency Research Lab at UFERSA and his main research interests are Microelectronics with focus in RFIC Design, Microwaves, Open-source Hardware and EDA, Instrumentation, AI, IoT and Embedded Systems. He has been an IEEE Member since 2007 and also member of SSC, MTT and CAS IEEE Societies. Currently He is member of the Technical Committee on the Open Source Ecosystem (TC-OSE) from IEEE Solid-State Circuits Society.